용력발광 전역 변형율 센서

Mechanoluminescence Full-Field Strain Sensor

윤 군 진*

* Associate Professor, Department of Civil Engineering, The University of Akron, Akron, OH, U.S.A.

1. Introduction

Mechanoluminescent materials can emit intense light in response of mechanical stress. They have increasingly received attentions for their potential applications to the full-field stress sensing of structures and active crack monitoring in the field of non-destructive testing (NDT) and structural health monitoring (SHM). Various applications of the ML materials have recently been demonstrated, for example, as stress sensors [Xu, Watanabe *et al.* (1999; Xu, Watanabe *et al.* (1999)], impact sensors [Chandra, Chandra *et al.* (2012)], damage sensors [Wang, Imai *et al.* (2011)], monitoring of the active cracks [Terasaki, Li *et al.* (2012)] and visualizations of stress distributions of solids [Kim, Kwon *et al.* (2007)], stress field near the crack tip [Kim, Kwon *et al.* (2003)], internal defect of pipes [Ono, Xu *et al.* (2010)], detecting fatigue cracks of pressure vessel [Ueno, Xu *et al.* (2013)] and fracture prediction in reinforced concrete [Chenshu LI, Chao-Nan XU *et al.* (2012)]. Many ML sensing materials have been developed and improved as potential ML stress sensors. Among them, $SrAl_2O_4:Eu^{2+}$ (SAOE) and $SrAl_2O_4:Eu^{2+}$, Dy^{3+} (SAOED) [Yamada, Fu *et al.* (2007)] are known to emit very intense light under mechanical loadings to the extent that the emission can be seen in day light with naked eyes. Therefore, these two materials are considered to be the most promising ML sensing materials for full-field stress sensing applications [Chandra and Chandra (2011)]. Although all of these applications are based upon a linear relationship between the ML light intensity and the applied stresses, recent studies indicate that a possible nonlinearity may exist between the ML light intensity and the applied stress [Yun, Rahimi *et al.* (2013)]. Rate-dependency of the ML light emission is a well-known characteristic of ML sensing materials [Kim, Kibble *et al.* (2009)].

The dynamic behavior of ML under cyclic loadings has been studied and ML response lagging has been reported by Sohn *et al.* [Sohn, Park *et al.* (2014)]. They concluded that, as the frequency increased, the decay rate increased dramatically which shows higher frequencies facilitate the consumption of the trapped carriers. Kim and Kim utilized ML paint to measure the torque applied to a transmission shaft and studied the dynamic torsional response of the ML sensor [Kim and Kim (2014)]. The ML light intensity was measured by a photomultiplier tube (PMT) sensor and converted to output

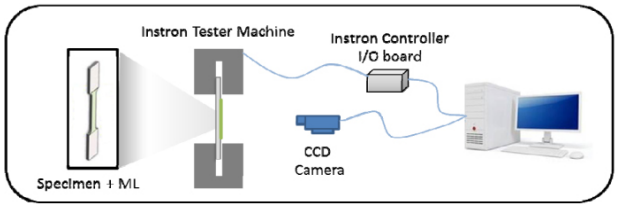

Figure 1 Schematic experimental test setup and configuration

voltages in their study. They have also proposed a new simple empirical calibration equation that expresses the ML intensity as a function of the applied torque and the torque rate. Constants in the calibration equation were determined by using a genetic algorithm. There are several influencing factors that can affect the ML intensity such as strain rates, stresses, photoexcitation power, and material concentration. Someya *et al.* suggested an idea of using two time constants (i.e. rise and decay) [Someya, Ishii *et al.* (2013)]. They indicated a linear relationship between the light intensity and the loading based on solely compression test data of bulk SAOE composites. Conclusion from their study showed that the measured lifetimes were independent of the concentration and excitation powder. Recently, Timilsina, *et al.* used an accumulated ML intensity for their immunity to the effect of strain rates on measurable stresses for evaluating Mode-I and II stress intensity factors of SAOED materials [Timilsina, Lee *et al.* (2013)].

In this article, a summary of the recent research work by the author is presented. In the following, the test setup will be described and followed by experimental observations of the ML phenomena. A predictive ML transduction model will be introduced in Section 3. Finally, a calibration model will be proposed in Section 4 and the conclusions will be provided in Section 5.

2. ML sensing film and test setup

ML materials can be used as a full-field stress sensor if they are coated on the structure's surface. In order to manufacture a thin ML film, commercial SAOED powder was mixed with the commercial optical epoxy resin and thin ML sensing film with thickness of 0.02 inches was made by the doctor blade method. The mass ratio of the epoxy resin to the SAOED powder was selected as 3:1 and a magnetic stirrer was used to disperse the powder uniformly in the epoxy.

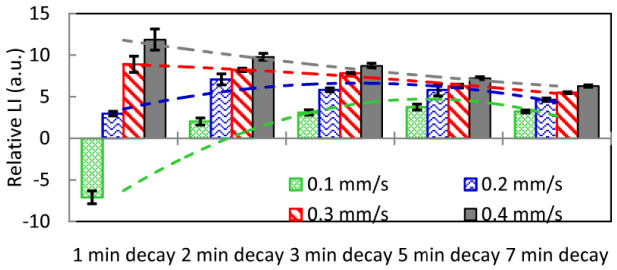

Figure 2 Change of relative ML light intensity for stress-free PL decay time intervals and strain rates (L.I.: Light Intensity)

A cut ML sensing film was bonded to standard dog-bone shaped aluminum (Al) specimens by using a commercial adhesive (M-Bond 200 from Micro-Measurements). During tension tests of the coated Al specimens, images were captured at a fixed frame per second by a CCD camera (AVT Manta G-033B) and National Instruments (NI) vision builder software. The CCD camera and controller of the Instron testing machine (220 kips) were synchronized to achieve a perfect coincidence between the captured images and the load step data by using an Instron digital input/output board. The experimental test setup is depicted in Figure 1.

3. Experimental observation of ML phenomena

ML phenomenon is complex due to many factors involved in transient changes of the ML light emission. In this article, stress, strain rate, stress-free PL decay time interval, stress-state PL decay and photoexcitation time were considered.

Figure 2 demonstrates changes of the relative ML light intensity for five different stress-free PL decay time intervals (1, 2, 3, 5, and 7 min) at four different strain rates (0.1, 0.2, 0.3, and 0.4 mm/s).

For each combination, three tests were repeated to minimize experimental errors and to evaluate the statistical variance as well as the mean values. The SAOED film samples were photoexcited for two minutes, aged in dark medium for different PL decay time intervals and then loaded to the fixed maximum force (15 kN) at different strain rates. As expected, the ML light emission increase with increase of strain rates, however, the change of ML light emission does not follow a simple pattern in terms of the change of PL decay time intervals. At the highest strain rate (0.4 mm/s), the

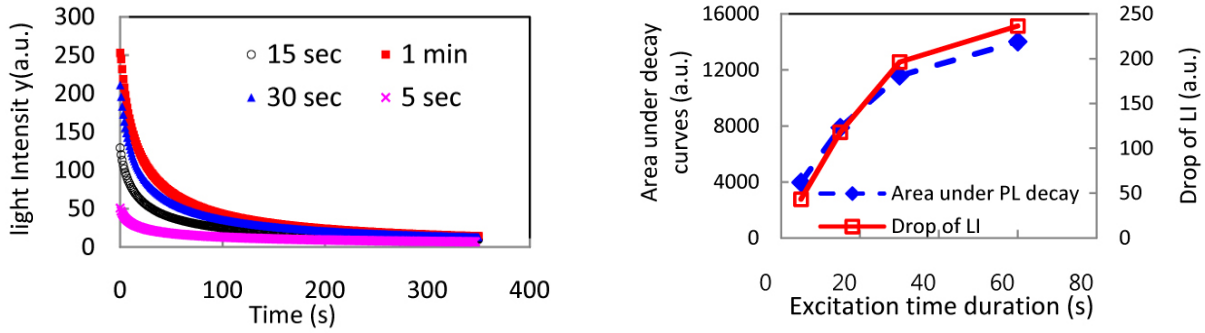

(a) (b)

Figure 3 Natural decay of PL decay of SAOED depending on photoexcitation times [Rahimi, Yun et al. (2013)]

ML sensitivity tends to decrease as the stress-free PL decay time interval increases whereas at the lowest strain rate (0.1 mm/s) the ML sensitivity tends to increase conversely.

Figure 3(a) demonstrates the stress-free PL decay curves of SAOED ML film subjected to four different excitation times. The results show that the stress-free PL decay is dependent on the duration of the photoexcitation, which has been previously reported [Pereyda-Pierre, Melendrez *et al.* (2011)]. Because the ML light emission of SAOED is strongly related to the PL decay characteristics, it is critical to take into account the PL decay of this material for a stress sensor. The drop of the PL intensity from 0 to 300 sec and areas under the stress-free PL decay versus photoexcitation times are plotted in Figure 3(b). For applications to ML stress sensors, the temporal changes of the PL decay must be considered because they significantly affect the relationship between the applied stress and the ML light intensity.

According to our experimental results, the behavior of PL decay under stress-states appears to be different from the stress-free PL decay. Instantaneous PL decay rate under a certain stress state was found to be increased rapidly in comparison to the stress-free PL decay rate. The stresses change instantly depending on instantaneous changes of the strain rate, therefore it is referred to as the instantaneous PL decay.

4. Predictive ML transduction model and verification based on experimental data

According to our experimental observations, a total light intensity (ΔI_t) is defined as a combination of the net ML light emission (ΔI_{ml}), stress-free PL decay (ΔI_{pl}) and additional stress-induced PL decay ($\Delta I'_{ml}$). With the exception of the stress-free PL decay, which is only dependent on the instantaneous light intensity ($I(t)$, See Figure 5), the light intensity changes are correlated to the stress level (σ) (i.e. time (t) in case of fixed strain rate), the strain rate ($\dot{\varepsilon}$) and the initial light intensity (I_0). The initial light intensity (I_0) can be uniquely determined as a function of the PL decay time interval (t_d) as long as the film is photoexcited consistently with a standard light source and an exposure time. Figure 4 indicates the contributions of the ML emission, the stress-free PL and the stress-state PL light decay to the total ML+PL light intensity schematically. According to the Figure 4, the total ML+PL light intensity from the ML film can be expressed as

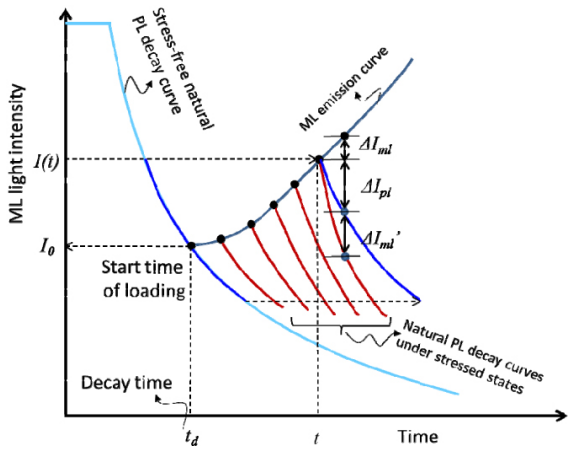

Figure 4 Stress–free PL decay curve, stress–state PL decay curves at different stress states and ML emission curve, and decompositions of instantaneous total ML+PL light intensity [Rahimi, Yun *et al.* (2013)]

$$I_t(I_0,\sigma,\dot{\varepsilon})_n = I_0 + \sum_{i=1}^{n}[\Delta I_{ml}(I_0,\sigma,\dot{\varepsilon})]_i + \sum_{i=1}^{n}[\Delta I_{pl}(I(t))]_i + \sum_{i=1}^{n}[\Delta I'_{ml}(I_0,\sigma,\dot{\varepsilon})]_i \quad (1)$$

where I_0 is the initial light intensity at the onset of stressing; σ is the stress; $\dot{\varepsilon}$ is the strain rate; n is the total number of incremental time steps and I_t is the total ML+PL light intensity. By substituting ΔI with $\dot{I}\Delta t$, in which $\dot{I}$ is the first derivative of the light intensity with respect to time and Δt is the time step, Eq. (1) can be recast into the following format.

$$I_t(I_0,\sigma,\dot{\varepsilon})_n = I_0 + \sum_{i=1}^{n}(\Delta I_{ml})_i + \left|\sum_{i=1}^{n}(\dot{I}_{pl})_i\Delta t\right| + \left|\sum_{i=1}^{n}(\dot{I}'_{ml})_i\Delta t\right|$$
$$= I_{ml}(I_0,\sigma,\dot{\varepsilon}) + \left|\int_{t_d}^{t}\dot{I}_{pl}(I(t))d\tau\right| + \left|\int_{t_d}^{t}\dot{I}'_{ml}(I_0,\tau,\dot{\varepsilon})d\tau\right| \quad (2)$$

A comprehensive experimental test database was prepared under various conditions in order to derive predictive models that can simulate changes of I_{ml} and $\dot{I}'_{ml}$. Effects of the initial light intensity (I_0), the strain rate ($\dot{\varepsilon}$), and the stress level (σ) were incorporated into the predictive model. Multi Gene Genetic Programming (MGGP) [Searson, Leahy *et al.* (2010)] was employed to derive the model equations. Eq. (3) shows a predictive model equation for the net ML light intensity in terms of stress (σ), strain rate ($\dot{\varepsilon}$), and initial light intensity (I_0).

$$I_{ml}(I_0,\sigma,\dot{\varepsilon}) = I_0 + A_1\dot{\varepsilon} + A_2 I_0\sigma + A_3 I_0^{\,2}\dot{\varepsilon} + A_4 I_0\dot{\varepsilon}\sigma + A_5\dot{\varepsilon}\sigma^2 \quad (3)$$

The model constants are calibrated as A_1=0.7434, A_2=2.043×10^{-10}, A_3=7.948×10^{-8}, A_4=1.033×10^{-11} and A_5=3.358×10^{-16} by using the experimental data. Comparisons between the experimentally measured ML light intensity and predicted net ML show that the proposed model could accurately predict the ML emission.

A new predictive equation is developed to model the long-lasting stress-free PL decay for ML which is the function of the time as follows.

$$I_{pl}(t) = B_0 - B_1\exp\left(\exp\left(-\frac{C_1}{t}\right)\right) - B_2\exp\left(\exp\left(-\frac{C_2}{t}\right)\right) \quad (4)$$

where $I_{pl}(t)$ presents the stress-free PL decay; B_0, B_1, and B_2 are constants; t is time, and C_1 and C_2 are the decay time constants. Based on our experimental data, the constants are calibrated as B_0=752.2, B_1=241.6, B_2=34.88, C_1=10.04 and C_2=58.06. Advantage of this model is that PL decay both in the fast and slow decay phases can be modeled by a single model. Finally, the predictive model for $\dot{I}'_{ml}$, which is a function of initial light intensity (I_0), stress (σ) and strain rate ($\dot{\varepsilon}$) can be derived as

$$\dot{I}'_{ml}(I_0,\sigma,\dot{\varepsilon}) = K_1\dot{\varepsilon}\sigma^2(1-\dot{\varepsilon}) + K_2\sigma + K_3 I_0\dot{\varepsilon}\sigma \quad (5)$$

where calibrated coefficients are K_1=3.149×10^{-16}, K_2=-4.845×10^{-9} and K_3=1.449×10^{-9} in our model.

5. Calibration model and validation

In this section, a calibration equation is proposed to convert the ML light emission to the effective strain. The effective strain is a scalar value and is defined as follows

$$\varepsilon_e = \frac{\sqrt{2}}{3}\left[(\varepsilon_{11}-\varepsilon_{22})^2 + (\varepsilon_{22}-\varepsilon_{33})^2 + (\varepsilon_{33}-\varepsilon_{11})^2 + 6(\varepsilon_{12}^2+\varepsilon_{23}^2+\varepsilon_{31}^2)\right]^{\frac{1}{2}} \quad (6)$$

which ε_e is the effective strain and ε_{ij} is the component of the strain tensors. In order to provide a calibration equation, comprehensive tension tests have been conducted on a standard dog-bone shape Aluminum specimen coated with a thin SAOED film with a thickness of 0.03 inches. The specimen is photoexcited for two minutes and decayed in the dark medium for seven minutes thereafter. After the certain decay time intervals, loads were linearly applied up to 15 kN at five different strain rates (0.1, 0.2, 0.3, 0.4, and 0.5 mm/s). Each test was repeated three times to minimize the experimental error. During the loading period, images are captured by a CCD camera at a frame rate of 10 fps. After carrying out the image processing, an average value of the ML light intensity is calculated for each frame. The incremental values of Δt, ΔLI, and $\Delta\eta$ have been input to the MGGP model to predict the change of effective strain in each time step. The predictive change of the effective strain can be expressed as follows

$$\Delta\varepsilon_{e(n)} = C_1(\Delta t + \log|\Delta LI + \varepsilon_{e(n-1)}| - \log|\varepsilon_{e(n-1)}|) + C_2(\Delta LI + \log|\Delta t|)$$
$$+ C_3(\varepsilon_{e(n-1)} - \Delta\eta_n - \log|\Delta\eta_n|) + C_4 \quad (7)$$

where Δt is the incremental time, ΔLI is the change of the ML light intensity for each increment, and $\Delta\eta_n$ can be

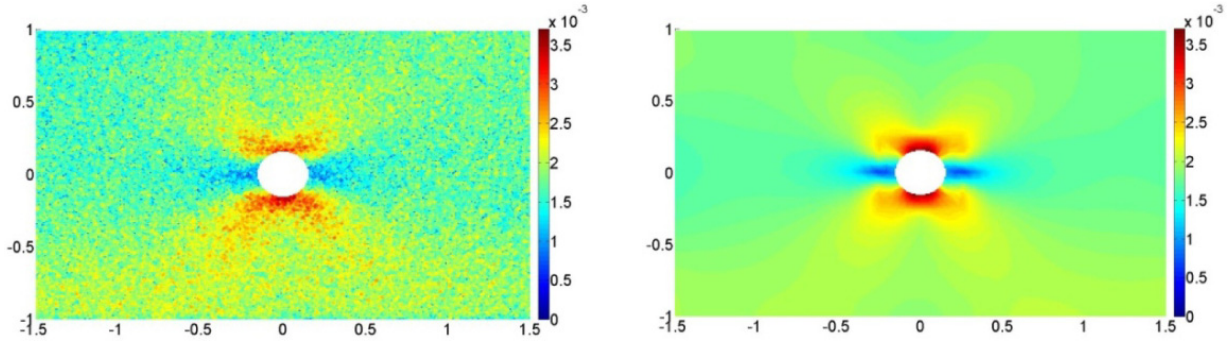

(a) (b)

Figure 5 Comparison of the ML effective strain and FE effective strain values

defined as $\Delta\eta_n=\Delta LI\varepsilon_{e(n-1)}$ for the nth increment. The model constants are calibrated as C_1=0.1, C_2=0.0859, C_3=0.01408, and C_4=0.1719. The effective strain in each step time can be obtained by accumulation of the changes of the effective strain values. To validate the performance of the calibration equation, a tension test has been conducted on a standard open-hole aluminum specimen coated with same thin ML film. Load was linearly applied up to 45 kN and the specimen was remained in the linear-elastic range. Figure 5 (a) shows the full-field effective strain distribution using the ML sensing film and the calibration model and Figure 5 (b) shows the effective strain values from the FE simulation (ABQUS 6.13-2). According to the Figure 5, the present calibration model could convert ML light intensity to the effective strain accurately and the results are validated with high accuracy.

6. Conclusion

In this article first, based on experimental testing of the SAOED thin film coated on aluminum specimens subjected to monotonically increasing tensile forces, ML phenomena were investigated considering the effect of the stresses, strain rates, and the PL decay time intervals on the ML light emission.

A predictive ML transduction model was proposed to predict the ML light intensity from SAOED thin-film coating sensor under mechanical loading. Mechanical energy applied to the ML sensing film was transduced to incremental change of the total light intensity which was subdivided to the net ML emission, the stress-free PL decay and the stress-state instantaneous PL decay. The predictive equations are derived based on the experimental test data. Finally, a calibration model is proposed to convert the net ML emission from the thin-film to the actual effective strain values. The effective strain values from ML calibration are then compared and validated with those from a FE analysis. The highly accurate results from this study shows that SAOED ML sensing films can be used as a new non-contact full-field strain sensor.

Acknowledgement

This research was possible by the supports from Ministry of Knowledge Economy (South Korea) through 2012 development of industry root technologies (IT-fusion). Author is grateful for their supports.

References

1. Chandra, B. P., V. K. Chandra, S. K. Mahobia, P. Jha, R. Tiwari and B. Haldar (2012). “Real-time mechanoluminescence sensing of the amplitude and duration of impact stress.” *Sensors and Actuators A: Physical*, vol. 173, no., pp.9-16.
2. Chandra, V. K. and B. P. Chandra (2011). “Suitable materials for elastico mechanoluminescence-based stress sensors.” *Optical Materials*, vol. 34, no. 1, pp.194-200.
3. Chenshu LI, Chao-Nan XU, Daisuke ONO, Naohiro UENO and Y. KAWABATA (2012). “Fracture Prediction in Reinforced Concrete Using Mechanoluminescent Sensor.” *Journal of JSEM*, vol. 12, no. Special Issue, pp.s205-s208.
4. Kim, G. W. and J. S. Kim (2014). “Dynamic torsional response analysis of mechanoluminescent paint and its application to non-contacting automotive torque transducers.” *Measurement Science & Technology*, vol. 25, no. 1, pp.
5. Kim, J. S., K. Kibble, Y. N. Kwon and K. S. Sohn (2009).

"Rate-equation model for the loading-rate-dependent mechanoluminescence of $SrAl_2O_4:Eu^{2+}$, Dy^{3+}." *Optics Letters*, vol. 34, no. 13, pp.1915-1917.

6. Kim, J. S., Y. N. Kwon, N. Shin and K. S. Sohn (2007). "Mechanoluminescent $SrAl_2O_4$:Eu, Dy phosphor for use in visualization of quasidynamic crack propagation." *Applied Physics Letters*, vol. 90, no. 24, pp.
7. Kim, J. S., Y. N. Kwon and K. S. Sohn (2003). "Dynamic visualization of crack propagation and bridging stress using the mechano-luminescence of $SrAl_2O_4$:(Eu,Dy,Nd)." *Acta Materialia*, vol. 51, no., pp.6437-6442.
8. Ono, D., C. N. Xu, C. Li and N. Bu (2010). "Visualization of Internal Defect of a Pipe Using Mechanoluminescent Sensor." *Journal of the Japanese Society for Experimental Mechanics*, vol., no. Special Issue, pp.152-156.
9. Pereyda-Pierre, C., R. Melendrez, R. Garcia, M. Pedroza-Montero and M. Barboza-Flores (2011). "Persistent luminescence and thermoluminescence of UV/VIS -irradiated $SrAl_2O_4$: Eu^{2+}, Dy^{3+} phosphor." *Radiation Measurements*, vol. 46, no. 12, pp.1417-1420.
10. Rahimi, M. R., G. J. Yun and J. S. Choi (2013). "A Predictive Mechanoluminescence Transduction Model for Thin Film $SrAl_2O_4:Eu^{2+}$, Dy^{3+} (SAOED) Stress Sensor." *Acta Materialia*, first revision submitted.
11. Rahimi, M. R., G. J. Yun, G. L. Doll and J. S. Choi (2013). "Effects of Persistent Luminescence on Mechanoluminescence Phenomena of $SrAl_2O_4:Eu^{2+}$, Dy^{3+} Materials." *Optics Letters*, vol. 38, no. 20, pp.193235.
12. Searson, D. P., D. E. Leahy and M. J. Willis (2010). GPTIPS: an open source genetic programming toolbox for multigene symbolic regression. *International MultiConference of Engineers and Computer Scientists 2010*, Hong Kong.
13. Sohn, K. S., W. B. Park, S. Timilsina and J. S. Kim (2014). "Mechanoluminescence of $SrAl_2O_4:Eu^{2+}$, Dy^{3+} under cyclic loading." *Optics Letters*, vol. 39, no. 6, pp.1410-1413.
14. Someya, S., K. Ishii, M. Saeki and T. Munakata (2013). "Lifetime-based measurement of stress using mechanoluminescence of $SrAl_2O_4:Eu^{2+}$." *Optics Letters*, vol. 38, no. 7, pp.1095-1097.
15. Terasaki, N., C. Li, L. Zhang and C. N. Xu (2012). *Active Crack Indicator with Mechanoluminescent sensing technique Detection of crack propagation on building*. Sensors Applications Symposium (SAS), 2012 IEEE, Brescia.
16. Timilsina, S., K. H. Lee, I. Y. Jang and J. S. Kim (2013). "Mechanoluminescent determination of the mode I stress intensity factor in $SrAl_2O_4:Eu^{2+}$, Dy^{3+}." *Acta Materialia*, vol. On-line, no., pp.
17. Ueno, N., C.-N. Xu and S. Watanabe (2013). "Fatigue Crack Detection of CFRP Composite Pressure Vessel Using Mechanoluminescent Sensor." *Sensors, 2013 IEEE*.
18. Wang, W. X., Y. Imai, C. N. Xu, T. Matsubara and Y. Takao (2011). "A New Smart Damage Sensor Using Mechanoluminescence Material." *Advanced Material Science and Technology*, Pts 1 and 2, 675-677, pp.1081-1084.
19. Xu, C. N., T. Watanabe, M. Akiyama and X. G. Zheng (1999). "Artificial skin to sense mechanical stress by visible light emission." *Applied Physics Letters*, vol. 74, no. 9, pp. 1236-1238.
20. Xu, C. N., T. Watanabe, M. Akiyama and X. G. Zheng (1999). "Direct view of stress distribution in solid by mechanoluminescence." *Applied Physics Letters*, vol. 74, no. 17, pp. 2414-2416.
21. Yamada, H., X. Y. Fu and C. N. Xu (2007). "Enhancement of adhesion and triboluminescent properties of $SrAl_2O_4$: Eu^{2+} films fabricated by RF magnetron sputtering and postannealing techniques." *Journal of the Electrochemical Society*, vol. 154, no. 11, pp.J348-J351.
22. Yun, G. J., M. R. Rahimi, A. H. Gandomi, G. C. Lim and J. S. Choi (2013). "Stress sensing performance using mechanoluminescence of $SrAl_2O_4$:Eu (SAOE) and $SrAl_2O_4$:Eu, Dy (SAOED) under mechanical loadings." *Smart Materials & Structures*, vol. 22, no. 5, pp. 055006.